Numerical investigation of the coupled mechanical behavior of self-healing materials under cyclic loading

J.A. Sanz-Herrera[a,*], A. Aliko-Benitez[a], A.M. Fadrique-Contreras[a]

[a] *School of Engineering, University of Seville*

Abstract

Self-healing structural materials are recognized as a cost effective and sustainable promising alternative to traditional maintenance methods of civil infrastructures. Great advances are being evidenced both in the synthesis/manufacturing and experimental characterization of these materials. However, there is limited information about reliable models which theoretically describe the observed behavior to be used as a useful design tool. In this paper a mechano-chemical-diffusive coupled model is introduced to represent the mechanical behavior of self-healing structural materials. Self-healing is restricted to precipitation of products within the matrix via an external agent, and is mathematically written by a set of reaction-diffusion equations. Mechanical behavior is modeled following classical continuous irreversible damage mechanics approaches. The overall model is numerically coupled and implemented in a finite element framework. The availability of the model is shown in the investigation of the self-healing mechanical behavior of a beam structure subjected to different regimes of cyclic loading – healing conditions.

*Corresponding author. Camino de los descubrimientos s/n, 41092 Seville, Spain. Tel.: +34 954 486079; fax: +34 954 487295

Email address: jsanz@us.es (J.A. Sanz-Herrera)

Keywords: Self-healing, Reaction-diffusion equations, Damage mechanics, Finite Element Method, Computational mechanics

1. INTRODUCTION

Self-healing materials are a class of artificial materials that mimics the autonomous repairing capability of natural materials, such as animal tissues or organs. This concept has been transferred and investigated in engineering materials, namely, alloys, concrete or biomaterials, due to the great potential they offer in the referred applications (Li and Yang, 2007a,b).

In the case of concrete, the potential of self-healing capability is prominent both in economic and sustainability terms: In USA, bridge repairing and maintenance is estimated in 200 billion dollars by Breugel (2007), whereas rebuilding of deficient constructions is estimated in 2000 billion dollars by Broek (2009). Overall, the costs of repairing and maintenance of civil engineering infrastructures is estimated in 50% of the total budget of this item in western countries (Broek, 2009). It is then clear the interest of the scientific community in the research and development of structural materials with autonomous healing features, as evidenced in the number of publications in this field in the past years (Neville, 2002; Li and Yang, 2007a,b).

Self-healing structural materials have been successfully synthesized in the laboratory in the last decades. The most promising healing mechanisms are based on (i) bacterial activity within the cement matrix and (ii) precipitation of products within the damaged matrix via reaction with an external agent (Joseph et al., 2011; Seifan et al., 2016; Gupta et al., 2017). The most feasible techniques of subgroup (ii) are: Further hydration of non-hydrated cement

particles and formation of calcium precipitates (Schlangen, 2010). On the other hand, it has been evidenced that Engineered Cementitious Composites (ECC) is a well-suited base material as a self-healing concrete product (Li, 1998; Li et al., 2001; Li, 2003), due to its capacity to undergo a ductile behavior and to develop small distributed cracks in the matrix of the order of 50 mm. This crack size is ideal to be self-healed due to limited feasibility of self-healing mechanisms to repair larger cracks (Kenneth and Floyd, 1956; Jacobsen, 1998; Edvardsen, 1999; Yang et al., 2009).

Self-healing capability of structural materials has been largely tested in the laboratory. Direct experiments involve loading/unloading mechanical tests combined with healing cycles (Granger et al., 2007; Qian et al., 2010; Yang et al., 2011; Ma et al., 2014; Garcia et al., 2017), to cite a few. Healing is computed then as the recovery of mechanical properties such as flexural rigidity or stiffness. On the other hand, indirect experiments estimate healing indirectly through different indicators such as crack closure (Wiktor and Jonkers, 2011), acoustic emission analysis (Granger et al., 2007) or permeability tests (Reinhardt and Jooss, 2003; Honma et al., 2009; Lepech and Li, 2009; Sahmaran and Li, 2009; van Tittelboom et al., 2012; Ma et al., 2014; Dong et al., 2017).

There exists limited information about the mathematical modeling of self-healing structural materials. A continuum phenomenological model for self-healing in structural materials, e.g. concrete, may include an irreversible damage modeling followed by a certain evolution law for the healing variable, attending to the specifically modeled self-healing mechanism. Non-recoverable (irreversible) damage in concrete has been extensively studied

and there are several consistent models in the literature (Loland, 1980; Cook and Chindaprasirt, 1981; Redon and Chermant, 1999; Boussa et al., 2001; Tao and Phillips, 2005; Lai et al., 2009; Kim and Abu, 2011). These models are based on the Continuum Damage Mechanics (CDM) classical theory (Kachanov, 1958; Rabotnov, 1969; Lemaitre and Chaboche, 1990). As an extension of the referred models, self-healing in structural materials has been modeled phenomenologically (Remmers and de Borst, 2008; Adam, 1999; Darabi et al., 2012; Hilloulin et al., 2014). Some models were developed for non-autogenous healing mechanisms (Barbero et al., 2005), whereas specifically-based autogenous healing models have been developed for specific types of healing processes (Miao et al., 1995; Huang et al., 2013). On contrary, there is a lack of information in the literature about the numerical development and computational implementation of self-healing models with coupled physics.

In this paper, the numerical coupling between mechanical and healing problems is developed. The overall numerical multiphysics model is valid to capture the cyclic loading/unloading – healing regime of self-healing materials from a continuum perspective. In general terms, the model is available to simulate actual self-healing structures subjected to random cycles of loading and healing periods. The paper is organized as follows: First the mechanical and healing problems are introduced both in their theoretical and numerical forms. Then, the numerical coupling between the models is explained in a finite element framework. In the results section, a numerical investigation about the evolution of the cyclic behavior of a self-healing beam specimen is conducted. Finally, some conclusions are drawn at the end of the paper.

2. MECHANICAL MODELING

2.1. Theory

The model is established within the Continuous Damage Mechanics (CDM) theory under the strain equivalence hypothesis (Lemaitre and Chaboche, 1990). Then, an idealized macroscopic configuration is adopted such that $\boldsymbol{\varepsilon}$ and $\boldsymbol{\sigma}$ are referred as the effective strain and stress quantities, respectively. The relationship between effective strain and stress tensors is given by,

$$\dot{\boldsymbol{\sigma}} = \boldsymbol{D} : \dot{\varepsilon} \tag{1}$$

$\boldsymbol{D}$ being the macroscopic effective tangent stiffness tensor, defined as,

$$\boldsymbol{D} = \frac{d\boldsymbol{\sigma}}{d\boldsymbol{\varepsilon}} \tag{2}$$

On the other hand, following the CDM approach $\boldsymbol{D}$ is related to the nominal (undamaged) configuration as follows,

$$\boldsymbol{D} = (1 - \phi) \cdot \boldsymbol{C} \tag{3}$$

where $\boldsymbol{C}$ is the linear stiffness tensor and ϕ the irreversible damage variable. It is considered an isotropic damage model such that ϕ is a scalar quantity.

Evolution of damage variable follows a rate-dependent damage model proposed by Darabi et al. (2012), and validated in the context of self-healing bituminous materials. It is written as follows,

$$\dot{\phi} = \Gamma^{vd} \left(\frac{Y}{Y_{th}} \right) (1 - \phi)^2 \exp(k \cdot \varepsilon_{eff}); \qquad Y = \sqrt{3J_2} \tag{4}$$

Γ^{vd} being the viscosity parameter of damage, and k a model parameter. $\boldsymbol{\varepsilon}_{eff} = \sqrt{\boldsymbol{\varepsilon}_{ij}\boldsymbol{\varepsilon}_{ij}}$ is the effective strain, Y_{th} the threshold damage force, and Y the driving force defined in Eq. (4). $J_2 = \frac{1}{2}s_{ij}s_{ij}$ is the second deviatoric stress invariant with $s_{ij} = \sigma_{ij} - \frac{1}{3}\sigma_{kk}\delta_{ij}$ the deviatoric stress tensor and δ_{ij} the Kronecker delta (Darabi et al., 2012).

The viscodamage (non-recoverable) surface f^{vd} is defined from Eq. (4):

$$f^{vd} = \frac{Y}{Y_{th}}(1-\phi)^2 exp(k \cdot \varepsilon_{eff}) - \frac{\dot{\phi}}{\Gamma^{vd}} \leq 0 \tag{5}$$

The irreversible damage variable ϕ evolves according to (4) once the damage surface becomes equal or greater than zero. The numerical implementation of the presented damage model is explained in the next section in the framework of the Finite Element Method (FEM).

The uniaxial mechanical behavior of the presented damage model can be seen in Fig. 1, for a loading–unloading–loading cycle with strain velocity $5 \cdot 10^{-3} s^{-1}$. The plot is shown for different model shape parameters. The rest of parameters of the model are given in Table 1.

2.2. Numerical implementation

The weak form of the CDM theory (in the absent of body forces) yield to the following expression (Bathe, 1996; Hughes, 2000; Reddy, 1993; Zienkiewicz and Taylor, 2000):

$$\int_{\Omega} \dot{\boldsymbol{\sigma}} : \delta\boldsymbol{\varepsilon} \; d\mathbf{X} = \int_{\Gamma} \dot{\mathbf{f}} \cdot \delta\mathbf{u} \; d\mathbf{X} \tag{6}$$

where time-derivative external forces $\dot{\mathbf{f}}$ fulfill equilibrium conditions with internal time-derivative stress tensor. Ω is the volume occupied by the domain

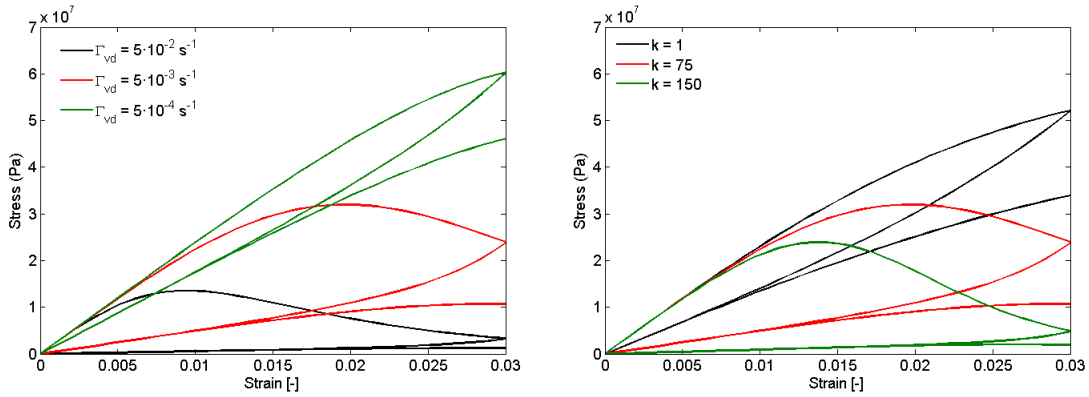

Figure 1: Uniaxial mechanical behavior of the damage model under a a loading–unloading–loading cycle. Left: Influence of Γ^{vd} shape parameter. Right: Influence of k shape parameter.

with boundary Γ. $\mathbf{X}$ is the vector position of a material point of the domain. On the other hand, $\delta\mathbf{u}$ is a virtual displacement field associated to a virtual strain tensor $\delta\boldsymbol{\varepsilon}$ through the compatibility operator:

$$\delta\boldsymbol{\varepsilon} = \frac{1}{2}\left(\nabla\delta\mathbf{u} + \nabla^T\delta\mathbf{u}\right) \tag{7}$$

By substitution of (1) and (3) into (6) yields:

$$\int_\Omega (1-\phi)\mathbf{C} : \dot{\boldsymbol{\varepsilon}} : \delta\boldsymbol{\varepsilon}\; d\mathbf{X} = \int_\Gamma \dot{\mathbf{f}} \cdot \delta\mathbf{u}\; d\mathbf{X} \tag{8}$$

The numerical FEM procedure is followed (Bathe, 1996; Hughes, 2000; Reddy, 1993; Zienkiewicz and Taylor, 2000): (i) time-derivative quantities are approached as (an implicit, unconditionable stable scheme is followed) $\dot{\square} = \frac{\Delta\square}{\Delta t}$, (ii) domain is decomposed into finite element domains Ω^e, such that $\int_\Omega \square d\mathbf{X} = \sum_{e=1}^{N_e}\left\{\int_{\Omega^e}\square d\mathbf{X}\right\}$, and (iii) displacements are approached by

means of shape function matrices $\mathbf{N}(\mathbf{X})$ over the element: $\mathbf{u}(\mathbf{X}) = \mathbf{N}(\mathbf{X}) \cdot \mathbf{U}$, $\delta\mathbf{u}(\mathbf{X}) = \mathbf{N}(\mathbf{X}) \cdot \delta\mathbf{U}$, with $\mathbf{U}$ and $\delta\mathbf{U}$ node-valued vectors at nodal positions of displacement and virtual displacement vectors, respectively.

Substitution of time and spatial discretization, as referred above, into Eq. (8) yields:

$$\mathbb{A}_{e=1}^{N_e} \left\{ \int_{\Omega^e} (1 - \phi_{t+\Delta t}) \cdot \mathbf{B}^T \cdot \mathbf{C} \cdot \mathbf{B} \; d\mathbf{X} \cdot \Delta\mathbf{U} - \int_{\Gamma^e} \Delta\mathbf{f} \cdot \mathbf{N} \; d\mathbf{X} \right\} = \mathbf{0} \tag{9}$$

where $\mathbf{B}$ is the gradient of the shape functions matrix and $\mathbb{A}$ the assembly operator.

Nonlinear Eq. (9) is solved by means of a Newton-Raphson iterative procedure, using the linearized form of the equation around a configuration $\Delta\mathbf{U}^i$,

$$D\mathbf{RE}(\Delta\mathbf{U}^i) D\mathbf{U}^{i+1} - \mathbf{RE}(\Delta\mathbf{U}^i) = \mathbf{0} \tag{10}$$

where index i refers to an unconverged Newton-Raphson iteration in Eq. (10). Residual term $\mathbf{RE}(\Delta\mathbf{U}^i)$ is defined as,

$$\mathbf{RE}(\Delta\mathbf{U}^i) = \mathbb{A}_{e=1}^{N_e} \left\{ \int_{\Omega^e} (1 - \phi_{t+\Delta t}) \cdot \mathbf{B}^T \cdot \mathbf{C} \cdot \mathbf{B} \; d\mathbf{X} \cdot \Delta\mathbf{U}^i - \int_{\Gamma^e} \Delta\mathbf{f} \cdot \mathbf{N} \; d\mathbf{X} \right\} \tag{11}$$

On the other hand, the tangent matrix $D\mathbf{RE}(\Delta\mathbf{U}^i)$ is defined in Eq. (10) as follows,

$$D\mathbf{RE}(\Delta\mathbf{U}^i) = \mathbb{A}_{e=1}^{N_e} \left\{ \int_{\Omega^e} (1 - \phi_{t+\Delta t}) \cdot \mathbf{B}^T \cdot \mathbf{C} \cdot \mathbf{B} \; d\mathbf{X} - \int_{\Omega^e} \mathbf{B}^T \cdot \mathbf{C} \cdot \mathbf{B} \otimes \frac{\partial \phi_{t+\Delta t}}{\partial \Delta\mathbf{U}^i} \; d\mathbf{X} \right\} \tag{12}$$

The derivative of the damage variable with respect to the increment of displacement vector is obtained following the chain's rule, according to the selected damage model in (4):

$$\frac{\partial \phi_{t+\Delta t}}{\partial \Delta \mathbf{U}} = \frac{\partial \phi_{t+\Delta t}}{\partial Y_{t+\Delta t}} \cdot \frac{\partial Y_{t+\Delta t}}{\partial \boldsymbol{\varepsilon}_{t+\Delta t}} \cdot \frac{\partial \boldsymbol{\varepsilon}_{t+\Delta t}}{\partial \Delta \mathbf{U}} + \frac{\partial \phi_{t+\Delta t}}{\partial \varepsilon_{eff,t+\Delta t}} \cdot \frac{\partial \varepsilon_{eff,t+\Delta t}}{\partial \boldsymbol{\varepsilon}_{t+\Delta t}} \cdot \frac{\partial \boldsymbol{\varepsilon}_{t+\Delta t}}{\partial \Delta \mathbf{U}} \quad (13)$$

After the assembly of Eq. (10), using Eqs. (11) and (12), and once convergence is achieved and hence $\Delta \mathbf{U}$ is obtained, displacement vector is computed as $\mathbf{U}_{t+\Delta t} = \mathbf{U}_t + \Delta \mathbf{U}$.

3. SELF-HEALING MODEL

3.1. Theory

The assumed self-healing mechanism is based on formation of a repairing agent in the interior of the material due to the reaction between an incoming (dynamic) species from the exterior and a (static) substance present in the material. The driving force of the mobile agent is assumed to be a fickean diffusion phenomenon in the presence of (damaged) cracked materials. Therefore, ions circulation along the material porosity due to solubility or conductivity factors are considered as a second order (negligible) diffusion phenomena. The referred reactive process may be simplified as follows,

$$D(aq) + S(s) \Leftrightarrow R(s) \quad (14)$$

D, $[\mathrm{mol}/m^3]$ being the diffusive (aqueous) species, S, $[\mathrm{mol}/m^3]$ the (solid) static reactant, and R, $[\mathrm{mol}/m^3]$ the (solid) repairing precipitated agent.

Note that the self-healing mechanism, generically described above, may represent at least two healing processes documented in the literature. First, crack closure due to calcium carbonate precipitation which in this case carbonate ions are the diffusive species, calcium the static one and calcium carbonate the repairing agent. On the other hand, healing due to further hydration of non-hydrated cement particles is another self-healing phenomenon available using this formulation: In this case the diffusive substance is water, the static one the non-hydrated cement and the repairing agent the hydrated cement after reaction.

The kinetics of the static species in (14) can be assumed as a first order kinetics similar to other works (Sanz-Herrera and Boccaccini, 2011; Aliko et al., 2015). Hence,

$$\dot{S} = -k_s \cdot S \cdot H[D] \tag{15}$$

being k_s $[1/s]$ the kinetic constant and $H[\bullet]$ the Heaviside function, introduced to take into account the availability of the reactant, and defined as,

$$H[\bullet] = \begin{cases} 1, & [\bullet] > 0 \\ 0, & [\bullet] = 0 \end{cases} \tag{16}$$

Taking into account the mass balance of (14), Eq. (15) yields,

$$\dot{R} = k_s \cdot S \tag{17}$$

Both diffusion and reaction are the sources of consumption of the dynamic species as follows,

$$\dot{D} = \dot{D}_{\text{diff}} + \dot{D}_{\text{reac}} = -k_d \cdot \nabla^2 D - k_s \cdot D \cdot H[S] \tag{18}$$

where right hand side of Eq. (18) was established using second Fick's law and mass balance in (14). Hence, k_d $[m^2/s]$ is the diffusion coefficient and ∇^2 the Laplacian operator.

Eqs. (15), (17) and (18) define the evolution of the species involved in the healing phenomenon. Their numerical implementation is shown in the next section.

3.2. Numerical implementation

The weak form of Eq. (18) can be written as follows,

$$\int_\Omega \dot{D} \cdot \delta D \, d\mathbf{X} + \int_\Omega k_d \cdot \nabla D \cdot \nabla \delta D \, d\mathbf{X} + \int_\Omega k_s \cdot D \cdot H[S] \cdot \delta D \, d\mathbf{X} = \int_\Gamma q \cdot \delta q \, d\mathbf{X} \tag{19}$$

where q is the normal flux to the boundary surface of substance D (according to first Fick's law). δD and δq are virtual concentration and normal flux of substance D, respectively. Following the analogous FEM time (an implicit, unconditionable stable scheme is followed) and spatial discretization than in section 2.2 (see Reddy (1993); Bathe (1996); Hughes (2000); Zienkiewicz and Taylor (2000)), and the approximation of variables over an element $D(\mathbf{X}) = \mathbf{N}(\mathbf{X}) \cdot \mathbf{D}$, $\delta D(\mathbf{X}) = \mathbf{N}(\mathbf{X}) \cdot \delta\mathbf{D}$, with $\mathbf{D}$ and $\delta\mathbf{D}$ node-valued vectors at nodal positions of concentration D and virtual concentration vectors, respectively. Hence,

$$\mathbb{A}_{e=1}^{N_e}\Big\{\frac{1}{\Delta t}\int_{\Omega^e}\mathbf{N}^T\cdot\mathbf{N}\;d\mathbf{X}\cdot\Delta\mathbf{D}+\int_{\Omega^e}\mathbf{B}^T\cdot k_d\cdot\mathbf{B}\;d\mathbf{X}\cdot\mathbf{D}_{t+\Delta t}+$$
$$+\int_{\Omega^e}\mathbf{N}^T\cdot k_s\cdot\mathbf{N}\;d\mathbf{X}\cdot\mathbf{H}[\mathbf{S}_{t+\Delta t}]*\mathbf{D}_{t+\Delta t}=\int_{\Gamma^e}q_{t+\Delta t}\cdot\mathbf{N}\;d\mathbf{X}\Big\}\quad(20)$$

where symbol $*$ in (20) denotes item by item (node by node) vector multiplication. Having into consideration $\mathbf{D}_{t+\Delta t}=\mathbf{D}_t+\Delta\mathbf{D}$, Eq. (20) can be written as follows,

$$\mathbb{A}_{e=1}^{N_e}\Big\{\int_{\Omega^e}\left(\frac{1}{\Delta t}\mathbf{N}^T\cdot\mathbf{N}+\mathbf{B}^T\cdot k_d\cdot\mathbf{B}\right)d\mathbf{X}\cdot\Delta\mathbf{D}+\int_{\Omega^e}\mathbf{N}^T\cdot k_s\cdot\mathbf{N}\;d\mathbf{X}\cdot\mathbf{H}[\mathbf{S}_{t+\Delta t}]*\Delta\mathbf{D}=$$
$$=\int_{\Gamma^e}q_{t+\Delta t}\cdot\mathbf{N}\;d\mathbf{X}-\int_{\Omega^e}\mathbf{B}^T\cdot k_d\cdot\mathbf{B}\;d\mathbf{X}\cdot\mathbf{D}_t-\int_{\Omega^e}\mathbf{N}^T\cdot k_s\cdot\mathbf{N}\;d\mathbf{X}\cdot\mathbf{H}[\mathbf{S}_{t+\Delta t}]*\mathbf{D}_t\Big\}\quad(21)$$

Eq. (21) can be written in a condensed matrix form as,

$$\mathbf{K}_{1D}\cdot\Delta\mathbf{D}+\mathbf{K}_{2D}\cdot\mathbf{H}[\mathbf{S}_{t+\Delta t}]*\Delta\mathbf{D}=\mathbf{Q}_{D,t+\Delta t}-\mathbf{F}_{1D,t}-\mathbf{F}_{2D,t}\qquad(22)$$

being,

$$\begin{aligned}\mathbf{K}_{1D}&=\mathbb{A}_{e=1}^{N_e}\left\{\int_{\Omega^e}\left(\frac{1}{\Delta t}\mathbf{N}^T\cdot\mathbf{N}+\mathbf{B}^T\cdot k_d\cdot\mathbf{B}\right)d\mathbf{X}\right\}\\ \mathbf{K}_{2D}&=\mathbb{A}_{e=1}^{N_e}\left\{\int_{\Omega^e}\mathbf{N}^T\cdot k_s\cdot\mathbf{N}\;d\mathbf{X}\right\}\\ \mathbf{Q}_{D,t+\Delta t}&=\mathbb{A}_{e=1}^{N_e}\left\{\int_{\Gamma^e}q_{t+\Delta t}\cdot\mathbf{N}\;d\mathbf{X}\right\}\\ \mathbf{F}_{1D,t}&=\mathbb{A}_{e=1}^{N_e}\left\{\int_{\Omega^e}\mathbf{B}^T\cdot k_d\cdot\mathbf{B}\;d\mathbf{X}\cdot\mathbf{D}_t\right\}\\ \mathbf{F}_{2D,t}&=\mathbb{A}_{e=1}^{N_e}\left\{\int_{\Omega^e}\mathbf{N}^T\cdot k_s\cdot\mathbf{N}\;d\mathbf{X}\cdot\mathbf{H}[\mathbf{S}_{t+\Delta t}]*\mathbf{D}_t\right\}\end{aligned}\qquad(23)$$

Applying again discretization of variables and explicit time discretization in Eqs. (15) and (17), such that $S(\mathbf{X}) = \mathbf{N}(\mathbf{X}) \cdot \mathbf{S}$ and $R(\mathbf{X}) = \mathbf{N}(\mathbf{X}) \cdot \mathbf{R}$ with $\mathbf{S}$ and $\mathbf{R}$ node-valued vectors at nodal positions of concentrations S and R, respectively; the following expressions are found,

$$\Delta\mathbf{S} = -\Delta t \cdot k_s \cdot \mathbf{S}_t * \mathbf{H}[\mathbf{D}_t] \tag{24}$$

$$\Delta\mathbf{R} = \Delta t \cdot k_s \cdot \mathbf{S_t} \tag{25}$$

Eqs. (21), (24) and (25) define the set of numerical equations of the healing model to be solved . After solution $\Delta\mathbf{D}$, $\Delta\mathbf{S}$, $\Delta\mathbf{R}$ are obtained, and variables are then updated as $\mathbf{D}_{t+\Delta t} = \mathbf{D}_t + \Delta\mathbf{D}$, $\mathbf{S}_{t+\Delta t} = \mathbf{S}_t + \Delta\mathbf{S}$ and $\mathbf{R}_{t+\Delta t} = \mathbf{R}_t + \Delta\mathbf{R}$. Remark on the slight nonlinearity that appears in Eq. (22) as consequence of the term $\mathbf{H}[\mathbf{S}_{t+\Delta t}]$. It is circumvented, sequentially, as follows: (1) Assume $H_i[S_{i,t+\Delta t}] = 1$ at all nodes, with index i referring to a nodal value; (2) solve Eqs. (22), (24), (25) and obtain nodal values D_i, S_i, R_i; (3) if D_i becomes negative at node i then repeat and go to item (2) considering $H_i[S_{i,t+\Delta t}] = 0$ for the referred node.

4. COUPLED NUMERICAL IMPLEMENTATION

Healing variable h may be defined as follows,

$$h = \frac{V_h}{V_D} \tag{26}$$

where V_h is the healed volume amount of the damaged volume V_D. Then h ranges from $0 \leq h \leq 1$, 0 meaning no healing whereas 1 completed healed

volume. In one hand, $V_D = \phi \cdot V$ according to classical CDM definition (Kachanov, 1958; Rabotnov, 1969; Lemaitre and Chaboche, 1990).

On the other hand, and according to the assumed healing mechanism based on formation of a repairing agent in the interior of the material, the repaired volume V_h can be defined through the amount of the new formed agent R as follows (Aliko et al., 2015),

$$V_h = V_R = \frac{R \cdot V \cdot M(R)}{\rho_R} \tag{27}$$

where V is the volume of the sample, and $M(R)$, ρ_R the molecular weight $[kg/\text{mol}]$ and density $[kg/m^3]$ of the repairing agent R, respectively. Hence, healing variable in (26) is defined as follows,

$$h = \frac{R \cdot M(R)}{\phi \cdot \rho_R}, \qquad \phi > 0 \tag{28}$$

Note that Eq. (28) couples both the mechanical problem, through damage variable ϕ, and the healing problem through repairing agent R. This coupling is treated as a weakly coupled problem by assuming that time t in a loading cycle (which may be of the order of seconds) is much lower than time T in the healing (repairing) cycle (which may be of the order of days for the assumed healing mechanism). Under this premise, mechanical problem of section 2 is solved for a loading cycle from $t_i \leq t \leq t_i + t_f$, and healing problem of section 3 is solved for a healing cycle from $T_j \leq T \leq T_j + T_f$. Note that both t_f and T_f may be different from cycle to cycle in the case that loading and healing cycles are different (or even random) along time. The coupling between both problems is explained next.

The numerical coupling between the mechanical and the healing problem

is illustrated in fig. 2: The analysis considers first an undamaged specimen with initialized damage to 0. Then, the specimen is loaded according to a certain loading cycle m. After this loading cycle damage variable ϕ is recorded, once the mechanical problem is solved. After a loading cycle, either another loading cycle or healing cycle may proceed. If a healing cycle follows, damage variable is collected at the end of the loading cycle, ϕ_{tf}, as an input argument for the healing problem. After the solution of the healing problem along the healing cycle n, healing variable is recorded. Then, after a healing cycle, either another healing cycle or loading cycle may proceed. If a loading cycle follows, damage variable at the end of the healing cycle, ϕ_{TF}, is updated according to $\phi_{TF} = \phi_{tf} \cdot (1 - h_{TF})$, h_{TF} being the healing variable at the end of the healing cycle. It is assumed, as a hypothesis, that the healed region shows the same mechanical properties than the original material. Remark that damage variable, defined after the healing cycle, is no longer irreversible (as in classical CDM), but it is reversible as consequence of healing/recovery phenomena and closure/repair of microscopic cracks. The new (reversible) damage is passed into the loading cycle mechanical problem as an initial condition of this variable.

The scheme shown in Fig. 2 is numerically implemented in a finite element framework using the software Abaqus 6.13. Therefore, both the mechanical problem and the healing one were implemented with the use of a UEL software independent subroutines. The coupling was implemented, following the flow diagram in Fig. 2, using Python-based language coding.

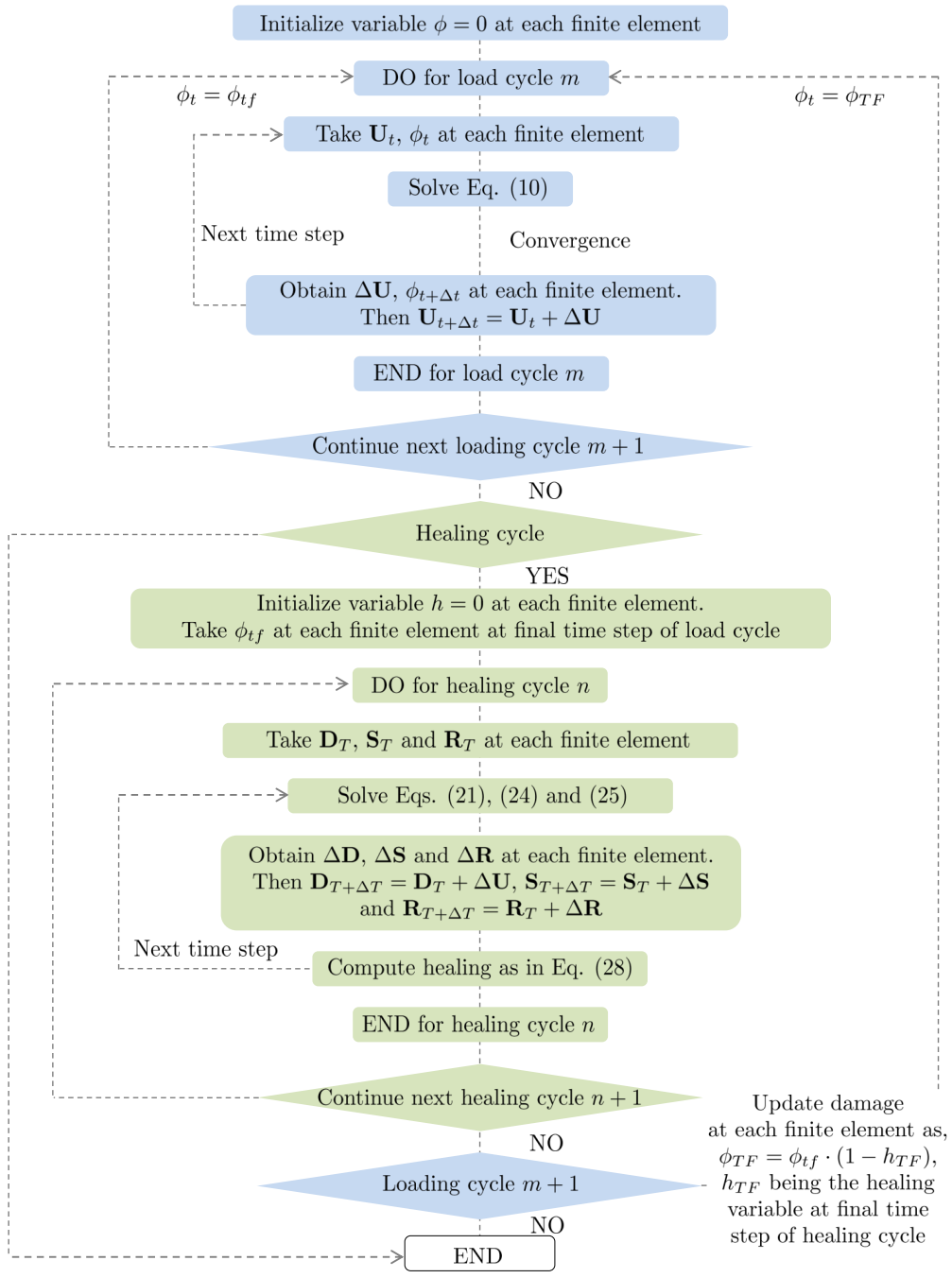

Figure 2: Flow diagram of the coupled mechanical–healing numerical algorithm. Colors blue and green referring to mechanical and healing problems, respectively.

5. RESULTS

5.1. Case study

The case study shown in this section considers the mechanical behavior evolution of a self-healing beam subjected to repetitive loading/unloading cycle followed by healing cycle. The self-healing capability is then numerically analyzed at different conditions.

The assumed healing mechanism in this example is based on precipitation of calcium carbonate (Aliko et al., 2015). Briefly, calcite formation is due to the reaction between the calcium ions Ca^{2+}, that are in the cement matrix, and the available bicarbonates (HCO_3^-) and carbonates (CO_3^{2-}) displaced in the cement matrix through diffusion. Those ions are available due to the enrichment of water in contact with the cement matrix with CO_2. These precipitates are mainly deposited on the crack surface as many experimental studies suggest (Cowie and Glassert, 1992; Edvardsen, 1999; Schlangen, 2010; Wiktor and Jonkers, 2011; Yang et al., 2011). So indirectly, the amount of calcite precipitates can be related to the capacity of the material to retrieve part of the accumulated damage. Then, in the theoretical model developed in section 3, D is $[CO_3^{2-}]$, S is $[Ca^{2+}]$ and R is $[CaCO_3]$. This healing mechanism is illustrated in Fig. (3).

A three-point bending test of a self-healing beam was selected for numerical simulations, see Fig. 4a, subjected to identical loading/unloading – healing cycles, see Fig. 4b, with displacement control. Mechanical properties of the beam, including damage model parameters (see section 2), are given in Table 1. Loading/unloading cycles are defined by the following set of parameters (see Fig. 4b): Loading/unloading deflection velocities are

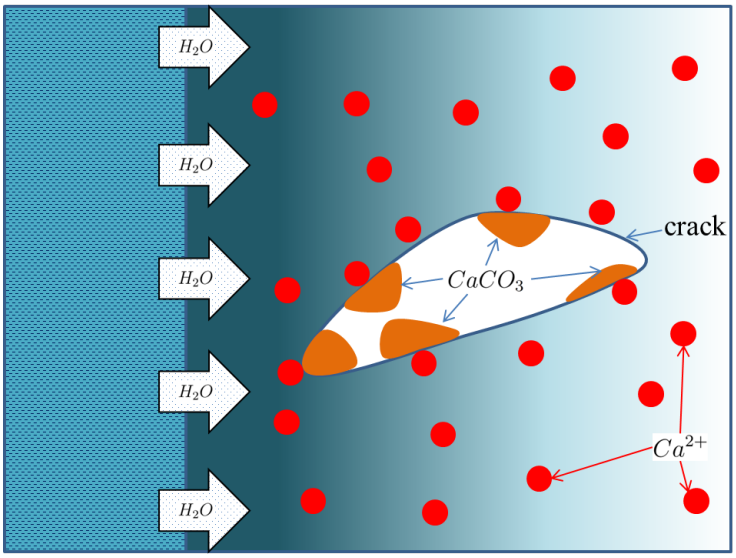

Figure 3: Healing mechanism model based on precipitation of calcium carbonate. Taken with permission from Aliko et al. (2015).

$\dot{v}_l = \dot{v}_u = 2\ mm/\text{min}$, loading/unloading times are equal $t_l = t_u$. 10 and 9 loading/unloading (damage) and healing cycles are considered, respectively. Moreover, maximum loading deflection $|v|$ is considered as a free parameter during the analysis.

Table 1: Damage model parameters (Darabi et al., 2012).

$E(GPa)$	ν	$\Gamma^{vd}(s^{-1})$	k	$Y_{th}(MPa)$
2	0.25	5×10^{-3}	75	2

On the other hand, healing model parameters are defined as $k_s = 1 \cdot 10^{-7}\ s^{-1}$ and $k_d = 1 \cdot 10^{-10} m^2/s$. Moreover, initial conditions and boundary conditions of species involved in the healing model are defined as dimension-

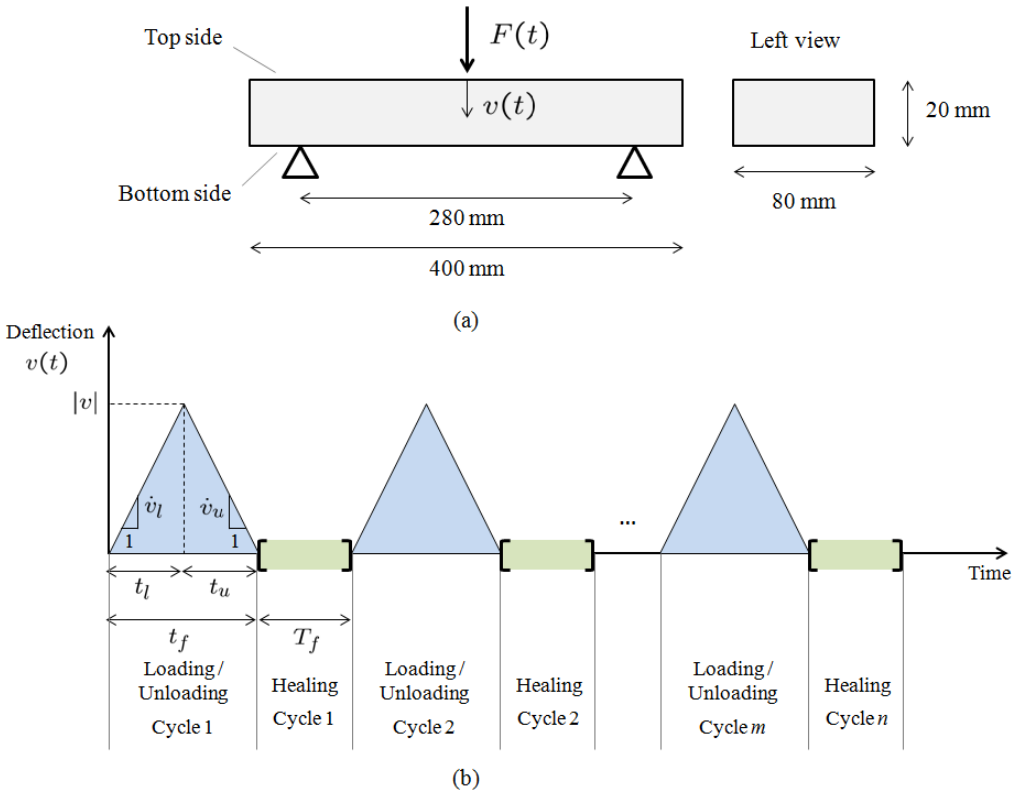

Figure 4: (a) Sketch of the case study selected for simulations. (b) Loading/unloading – healing cyclic regime.

less quantities as follows: A null concentration of carbonate $[CaCO_3]/[CO_3^{2-}](t = 0) = 0$ and a uniform calcium concentration $[Ca^{2+}]/[CO_3^{2-}](t = 0) = 0.3$ was considered at the interior domain of the beam. Moreover, a prescribed uniform carbonate concentration $[CO_3^{2-}]/[CO_3^{2-}] = 1$ on all boundary faces of the beam was assumed, in order to simulate contact with the (abundant) aqueous medium of the submerged beam structure. Therefore the healing cycle is assumed to be a certain time T_f which the beam is submerged in an aqueous solution, after a loading/unloading cycle. The aqueous solution is assumed to have the same density than water. These parameters of the healing model were used in a previous study and qualitatively validated with experimental works in Aliko et al. (2015). Moreover, healing cycle time T_f is considered as a free parameter during the analysis.

5.2. Cyclic behavior

Force–deflection cyclic behavior of the beam sketched in Fig. 4 is shown in Fig. 5. The plot is depicted for the different considered free parameters healing time T_f and magnitude of deflection $|v|$. The first initial loading/unloading cycle is highlighted in a different color in Fig. 5 as it is a common (initial) cycle for the different analyzed healing times. Note that, due to the deflection displacement control in the numerical experiments, the cyclic behavior converges in some cases to a certain path as the number of loading/unloading cycles increases. This phenomenon is explained next. On the other hand, it can be seen in Fig. 5 the beneficial trend of a longer healing time T_f since the force–deflection cyclic behavior is stiffer along time due to self-healing and recovering. Moreover, a larger magnitude of deflection $|v|$ induces higher damage in the specimen and hence softer force–deflection

curves as $|v|$ increases.

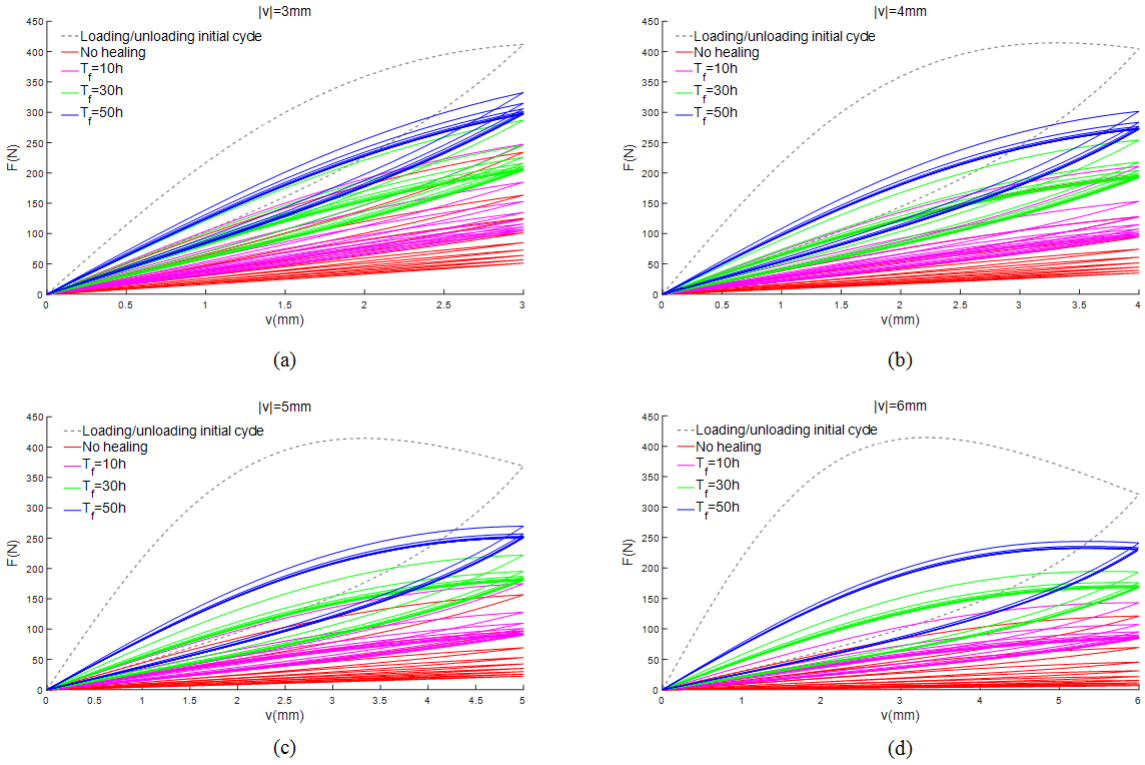

Figure 5: Force–deflection cyclic behavior in the three-point bending test for different healing times T_f. (a) $|v| = 3\ mm$, (b) $|v| = 4\ mm$, (c) $|v| = 5\ mm$ and (d) $|v| = 6\ mm$.

Fig. 6 shows damage and healing variables along loading/unloading (damage) and healing cycles, respectively, computed at bottom midpoint place of the beam, for different healing times T_f and magnitude of deflection displacement $|v|$. The figure is plotted in two-axis format such that damage variable is referred to the left axis during the damage cycle, and healing variable is referred to the right axis during the healing cycle. In Fig. 6 can be seen the recovery of damage as consequence of healing cycles for different duration,

from low to high recovery as healing time increases. The 'No healing' case turns into a continuous line along damage cycles, since loading/unloading conditions are applied without any healing cycle. Moreover, a larger magnitude of deflection $|v|$ along loading/unloading cycles imposes more severe damage conditions in the specimen as seen in Fig. 6. Moreover, damage variable is plotted in Fig. 7 for constant healing time $T_f = 50\ h$ as well as for monotonically ascending and descending healing times from healing cycle to cycle. In this case, monotonically ascending healing time is defined as $T_f = i \cdot \frac{50}{9}\ h$, for $i = 1..9$ healing cycles. On the other hand, monotonically descending healing time is defined as $T_f = (10 - i) \cdot \frac{50}{9}\ h$, for $i = 1..9$ healing cycles. Complementary to Fig. 6, Fig. 7 shows varying damage recovery from healing cycle to cycle for a reference healing time of $T_f = 50\ h$. In these simulations, ascending healing time converges to the constant healing time case, whereas the descending healing time converges to the no healing case as healing time diminishes with cycles.

Fig. 8 illustrates the ultimate bending force along loading cycles. The plot is depicted for the different considered free parameters healing time T_f and magnitude of deflection $|v|$. Fig. 8 shows a higher strength as healing times T_f increases, whereas a lower ultimate bending force is found for a higher magnitude of deflection loading. Note that the 'No healing' case shows a monotonically decreasing trend as loading/unloading cycles increases. This is due to the fact that the assumed damage model considers an additional damage during the unloading region, which explains the increase of damage during that period. On the other hand, for certain values of healing time and recovery, damage during unloading is balanced in the healing cy-

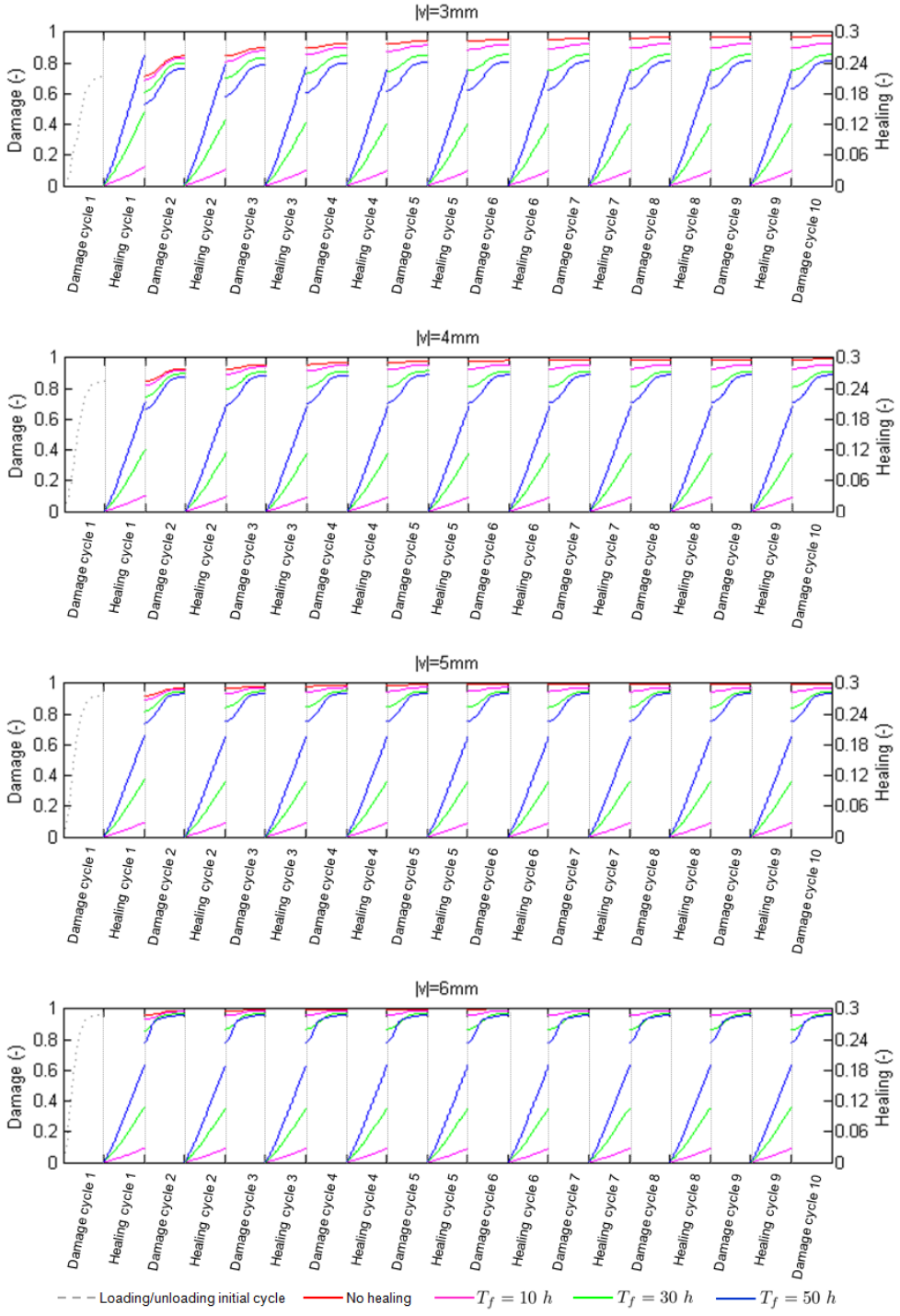

Figure 6: Damage (left axis) and healing (right axis) variables along loading/unloading (damage) and healing cycles, respectively, computed at bottom midpoint place of the beam, for different healing times T_f and magnitude of deflection displacement $|v|$. Damage and healing cycles abscissa axis was referred to the duration of the cycle in dimensionless form.

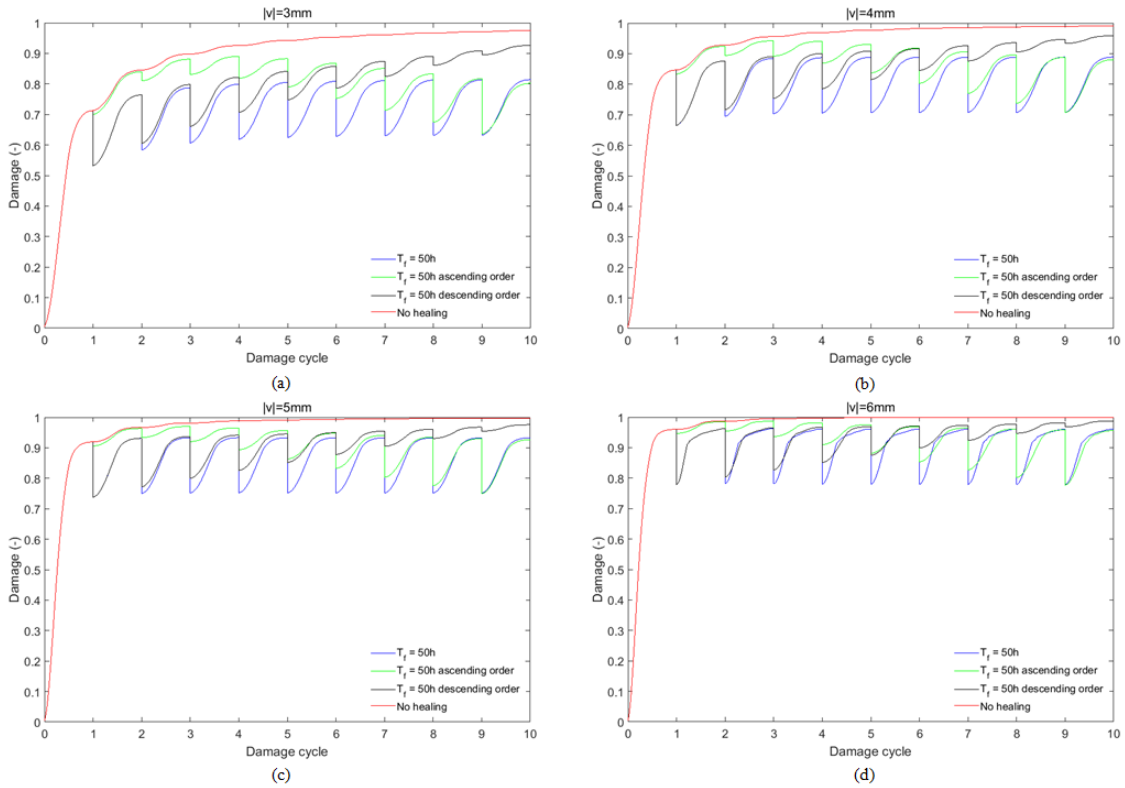

Figure 7: Damage variable along loading/unloading cycles computed at bottom mid-point place of the beam, for healing times $T_f = 50h$ (considering constant as well as monotonically ascending and descending healing time cycles) and magnitude of deflection displacement $|v|$: (a) $|v| = 3\ mm$, (b) $|v| = 4\ mm$, (c) $|v| = 5\ mm$ and (d) $|v| = 6\ mm$.

cle resulting in the convergence of the ultimate deflection force with along loading/unloading cycles. This phenomenon may be interpreted as a fatigue limit which exclusively appears in self-healing materials.

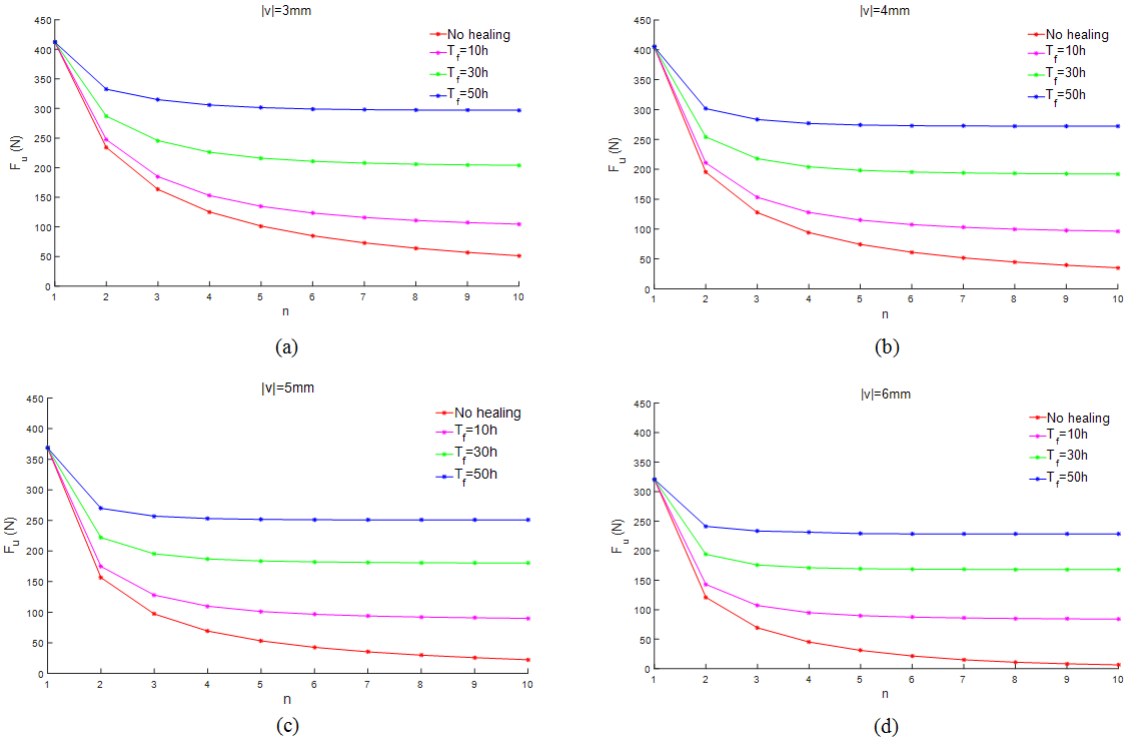

Figure 8: Ultimate bending force along loading cycles in the three-point bending test for different healing times T_f. (a) $|v| = 3\ mm$, (b) $|v| = 4\ mm$, (c) $|v| = 5\ mm$ and (d) $|v| = 6\ mm$.

5.3. Damage and healing

Damage and healing variables distribution along the beam specimen are shown in Figs. 9 and 10, respectively, for different healing times T_f and

magnitude of deflection displacement $|v|$. The figures are plotted at the end of the last loading/unloading (damage) cycle and end of last healing cycle, for damage and healing variables, respectively. The observed trend in previous figures for these parameters is given in Figs. 9 and 10. Note that healing, defined according to Eq. (28), increases when damage is low. It means, as seen in Fig. 10, that low damage regions are prone to recover and heal faster than those subjected to severe conditions of damage.

For completeness, variables associated to mechanical (damage) model and chemical-diffusive (healing) model are plotted in Figs. 11, 12 and 13. In one hand, mechanical minimum principal stresses and maximum principal stresses are plotted along the boundary of the beam specimen in Figs. 11 and 12, respectively. It is seen that higher values (magnitude) of minimum stresses and maximum stresses are given at the middle span of the top side (compressive bending side) and bottom side (tensile bending side) of the beam, respectively. In connection with damage plots (see Fig. 9), magnitude of minimum and maximum stresses decrease as damage increases. On contrary, magnitude of minimum and maximum stresses increase as damage decreases. This is a direct consequence of the definition of damage according to CDM: Overall and macroscopically, damage is directly related with the apparent stiffness of the material, hence stresses are concentrated in low damaged (stiffer) regions. Therefore, the trend of maximum and minimum stresses (magnitude) is inverse that the one followed by damage variable with free parameters healing times T_f and magnitude of deflection displacement $|v|$, as seen above.

On the other hand, dimensionless variables associated to calcium concen-

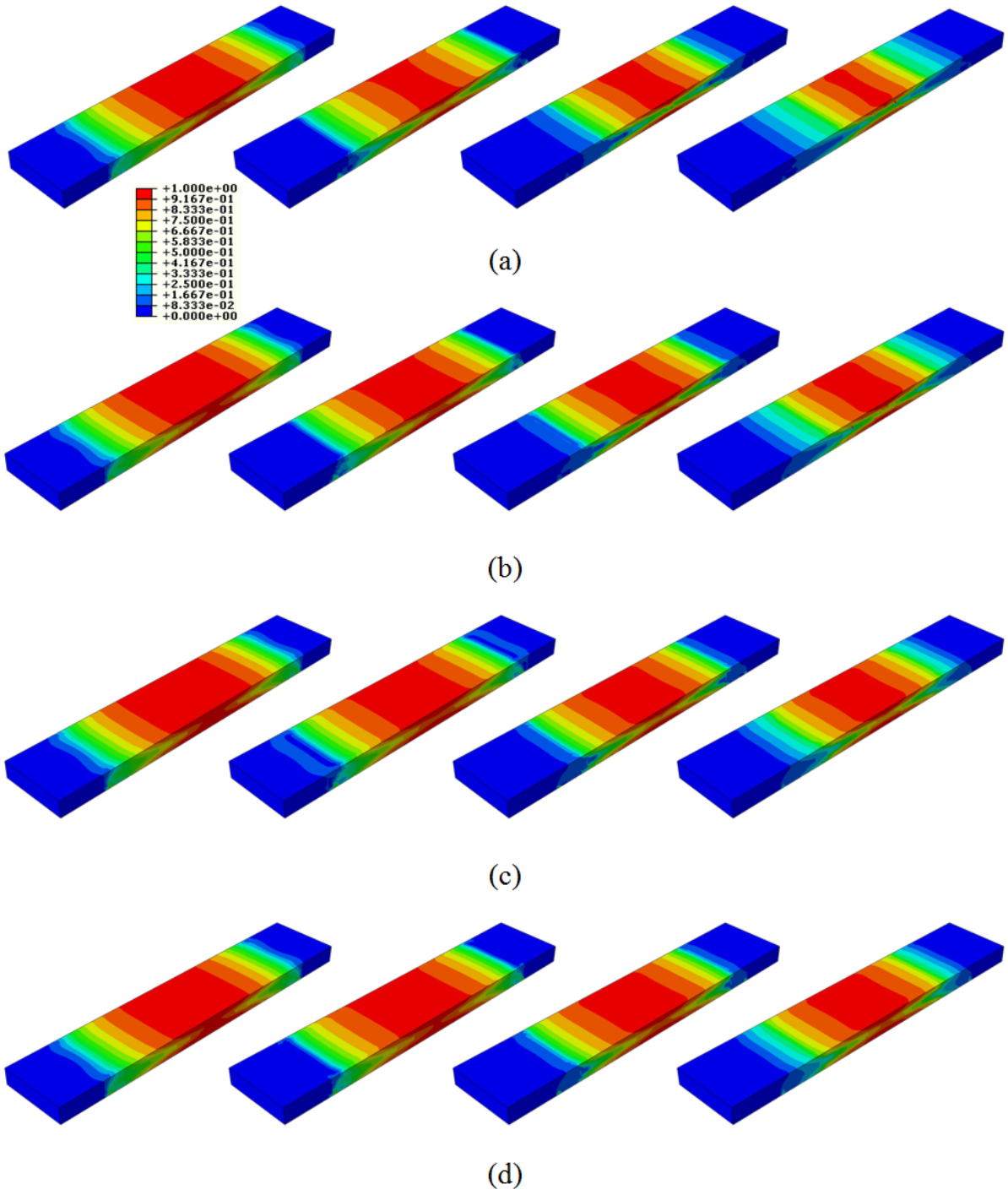

Figure 9: Damage variable, at the end of the last loading/unloading (damage) cycle, for different healing time T_f and magnitude of loading $|v|$. From left to right: No healing ($T_f = 0\ h$), $T_f = 10\ h$, $T_f = 30\ h$, $T_f = 50\ h$. (a) $|v| = 3\ mm$, (b) $|v| = 4\ mm$, (c) $|v| = 5\ mm$ and (d) $|v| = 6\ mm$.

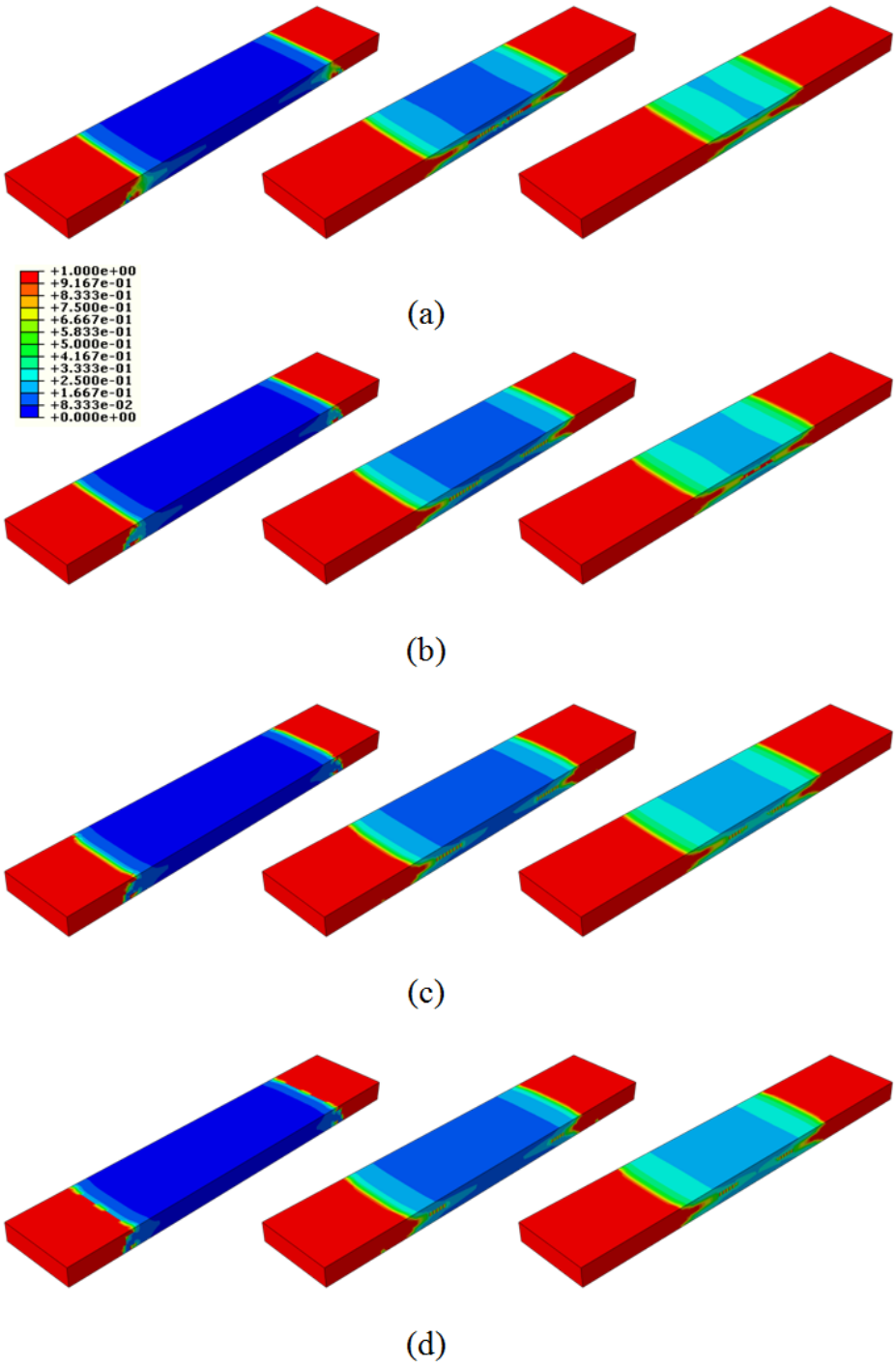

Figure 10: Healing variable, at the end of the last healing cycle, for different healing time T_f and magnitude of loading $|v|$. Left: $T_f = 10\ h$, middle: $T_f = 30\ h$, right: $T_f = 50\ h$. (a) $|v| = 3\ mm$, (b) $|v| = 4\ mm$, (c) $|v| = 5\ mm$ and (d) $|v| = 6\ mm$.

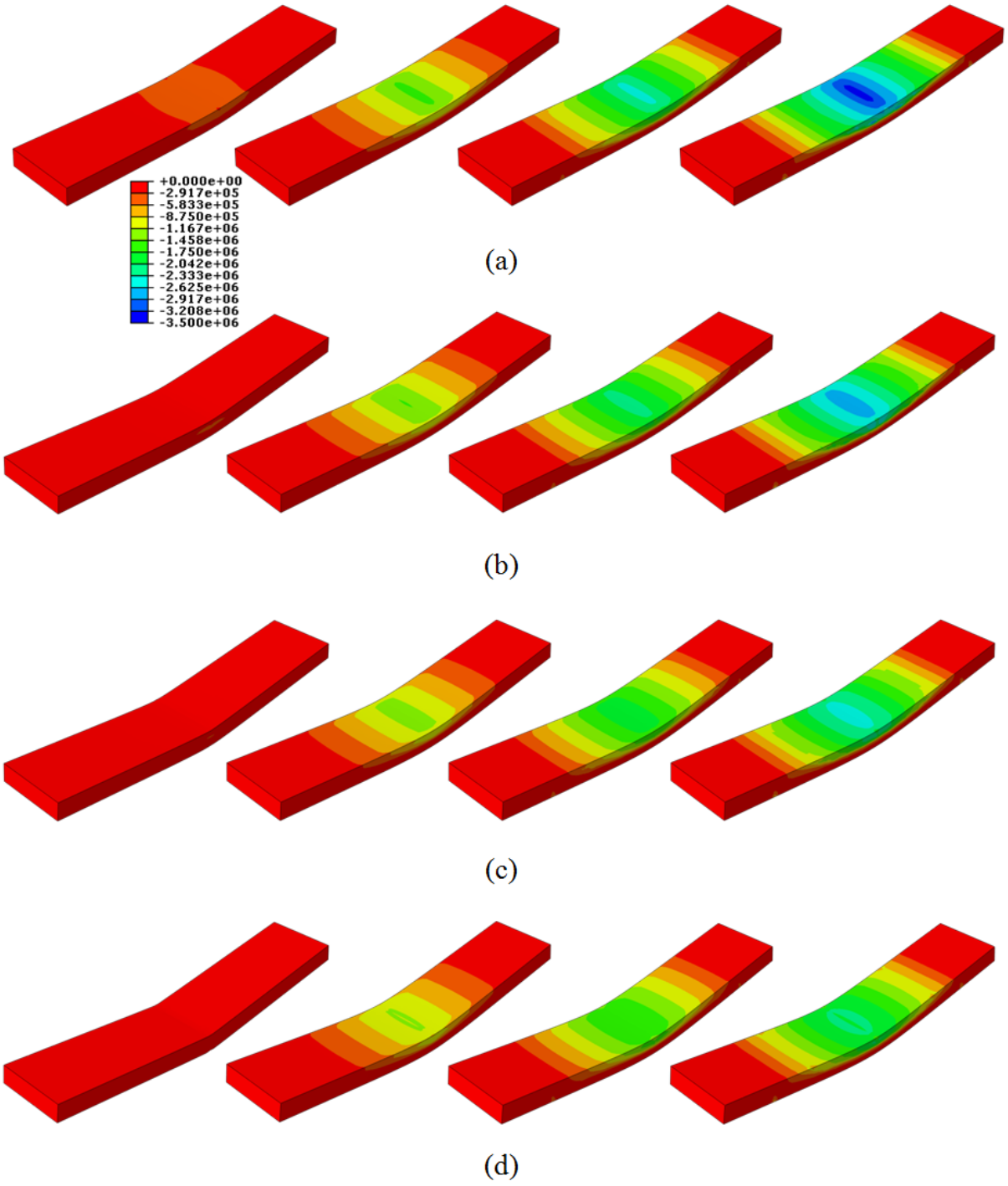

Figure 11: Minimum principal stress (N) at the top side perspective of the beam (see Fig. 4a) at the end of the last loading cycle (before unloading), for different healing time T_f and magnitude of loading $|v|$. From left to right: No healing ($T_f = 0\ h$), $T_f = 10\ h$, $T_f = 30\ h$, $T_f = 50\ h$. (a) $|v| = 3\ mm$, (b) $|v| = 4\ mm$, (c) $|v| = 5\ mm$ y (d) $|v| = 6\ mm$. Deformation scale factor $\times 3$.

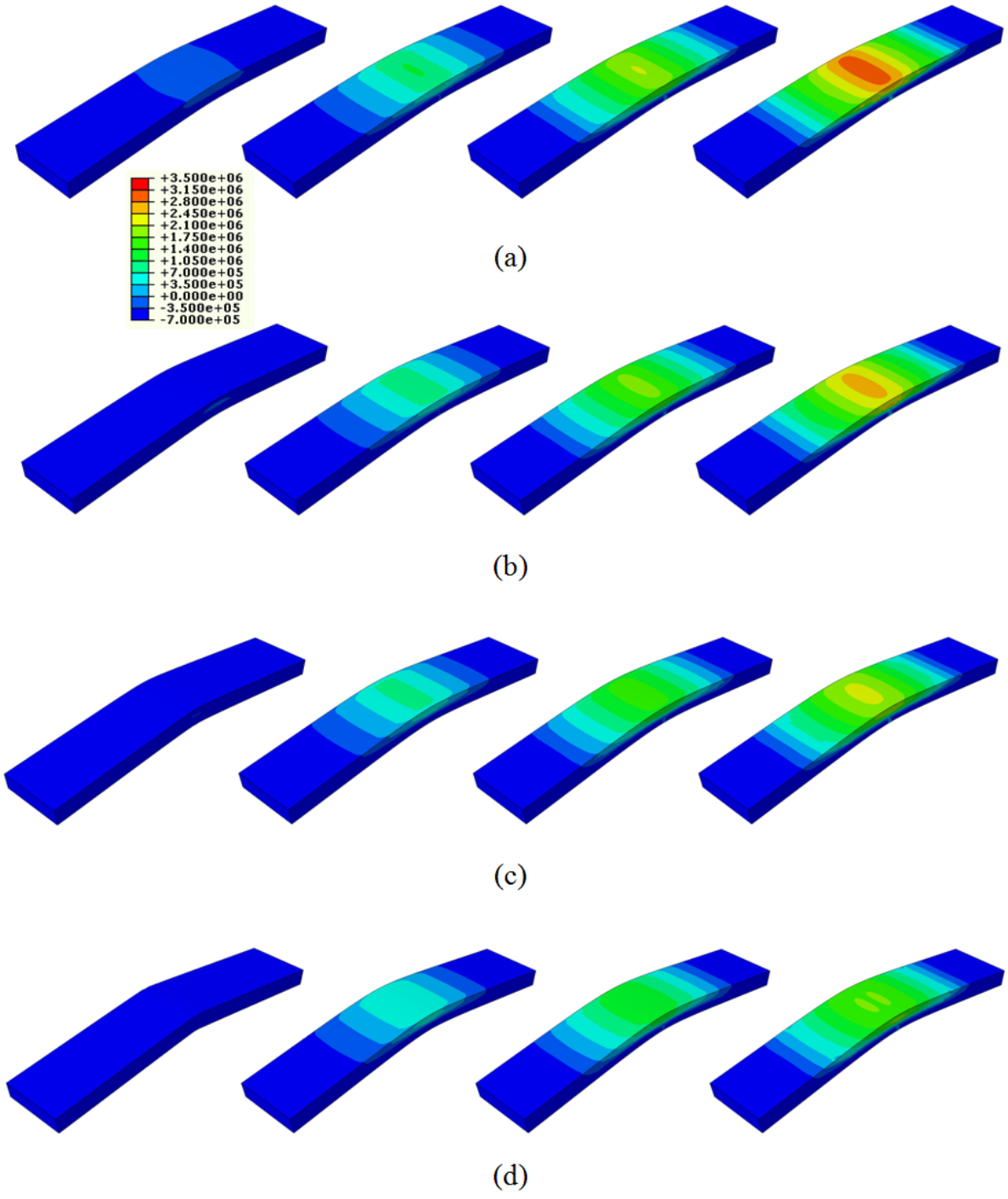

Figure 12: Maximum principal stress (N) at the bottom side perspective of the beam (see Fig. 4a) at the end of the last loading cycle (before unloading), for different healing time T_f and magnitude of loading $|v|$. From left to right: No healing ($T_f = 0\ h$), $T_f = 10\ h$, $T_f = 30\ h$, $T_f = 50\ h$. (a) $|v| = 3\ mm$, (b) $|v| = 4\ mm$, (c) $|v| = 5\ mm$ y (d) $|v| = 6\ mm$. Deformation scale factor $\times 3$.

tration, carbonate ions and production of calcium carbonate, are shown in Fig. 13. These concentrations, according to the chemical-diffusive model, are independent on the damage level and hence independent on magnitude of deflection $|v|$. Healing, according to its definition in Eq. (28), is the only variable related to damage in the model. Figs. 13a and 13b show the distribution at the boundary and interior of the beam (longitudinal midsection represented) of dimensionless calcium and carbonate, respectively, at the end of the last healing cycle and for different values of the healing time T_f. Both species are being depleted along the healing time as consequence of reaction and diffusion (carbonate) and reaction (calcium). On contrary, calcium carbonate variable precipitates, and hence giving place along healing time to the repairing agent which closes microcracks appeared in the material in the loading/unloading cycles (see Fig. 13c). Calcium carbonate variable, Fig. 13c, is plotted as well in dimensionless terms as the distribution at the boundary and interior of the beam (longitudinal midsection represented), at the end of the last healing cycle and for different values of the healing time T_f. The trend of these variables are (from boundary to the interior of the specimen): Increasing values of calcium due to higher availability of the reactant (carbonate) at the boundary (reaction and depletion), decreasing values carbonate due to diffusion from the boundary, and decreasing values of calcium carbonate due to higher availability of reactant (carbonate) at the boundary (precipitation and production).

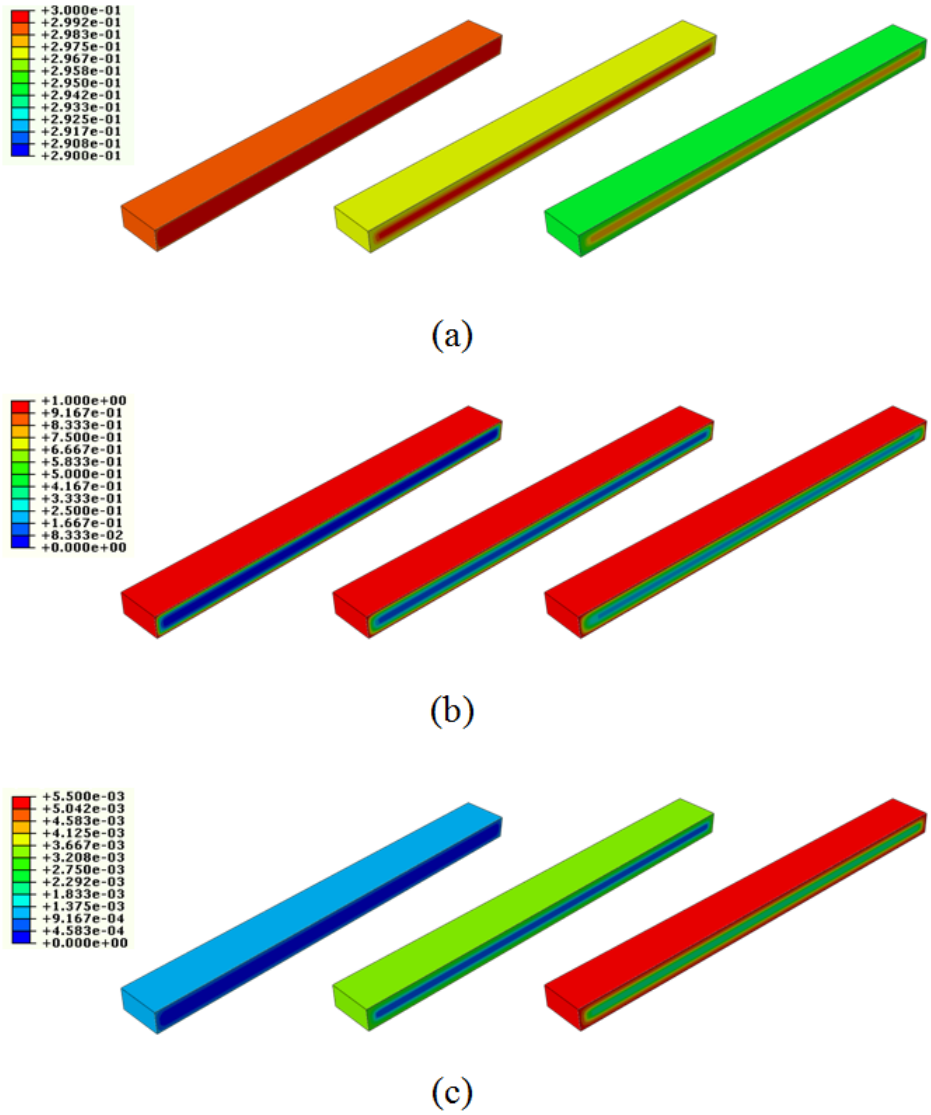

Figure 13: Variables of the chemical-diffusive model at the end of the last healing cycle, for different healing times T_f. longitudinal midsection represented. Left: $T_f = 10\ h$, middle: $T_f = 30\ h$, right: $T_f = 50\ h$. Dimensionless quantities of concentrations of (a) Calcium, (b) carbonate and (c) calcium carbonate.

6. CONCLUSIONS

A coupled mechano-chemical-diffusive model to simulate self-healing of structural materials has been proposed in this paper. In one hand, the model considers a thermodinamically consistent continuum damage model available for a self-healing structural material. On the other hand, a rationally based physico-chemical diffusive model has been used to describe self-healing phenomena. Even though self-healing model is restricted to precipitation of products via diffusion of an external agent, the formulation accounts for two important healing mechanisms that take place in structural materials, namely, precipitation of calcium carbonate and further hydration of cement particles within the cement matrix. The overall model turns into a weakly coupled model under the hypothesis that healing time is an order of magnitude higher than loading time, being this a feasible hypothesis at practical situations. A comprehensive numerical implementation, following a finite element framework, is detailed in this paper.

The global mechano-chemical-diffusive model introduces a number of model parameters due to the phenomenological continuum characteristic of the model. Nonetheless, each model parameter has a well-known physical meaning and can be measured in the laboratory with standard protocols. Even though the focus of the present work was the theoretical and numerical implementation of the self-healing phenomenon in structural materials, the proposed model needs experimental validation. This task is currently being performed as part of a research project.

Healing model variables, i.e. species concentrations, are independent of damage variable. Healing, according to its definition in Eq. (28), is the

only variable related to damage in the healing model. Actually, evolution of concentrations of species are related to the damage level in the sense that higher values of damage induce a more permeable microstructure (higher density of cracks) and hence ability of diffusive substances, i.e. carbonate, to react with defined species. The natural parameter of the healing model to consider this effect is taking a diffusion coefficient dependent on the level of damage, indirectly, through permeability. It was considered as uniform, as a first approach in the present work, being this is a limitation of the model.

The implemented model was investigated in the cyclic behavior of a self-healing beam subjected to loading/unloading – healing cycles. Results show higher recovery of mechanical properties for longer healing periods, as well as a softer behavior for high magnitude of loading. An important finding of the investigations was the appearance of a 'fatigue limit' at certain conditions of healing. This limit is a consequence of the self-healing feature of the material.

The proposed model may be a useful tool for continuum simulations and design of self-healing structures in the framework of cost-efficient and sustainable engineering materials.

REFERENCES

Adam, J.A., 1999. A simplified model of wound healing (with particular reference to the critical size defect). Math. Comput. Model. 30, 23-32.

Aliko-Benitez A., Doblare, M., Sanz-Herrera, J.A., 2015. Chemical-diffusive modeling of the self-healing behavior in concrete. Int. J. Solids Struct. 69-70, 392–402.

Bathe, K.J., 1996. Finite Element Procedures. Prentice-Hall, New Jersey.

Barbero, E.J., Greco, F., Lonetti, P., 2005. Continuum damage-healing mechanics with application to self-healing composites. Int. J. Damage Mech. 14, 51-81.

Boussa, H., Tognazzi-Lawrence, C., La Borderie, C., 2001. A model for computation of leakage through damaged concrete structures. Cem. Concr. Compos. 23, 279-287.

Breugel, KV., 2007. Is there a market for selfhealing cement-based materials?. Proceedings of the 1^{st} International Conference on Self-Healing Materials. Delft, Netherlands.

Broek, A.V., 2009. Self-healing concrete. Forbes Magazine 46–48.

Cook, D.J., Chindaprasirt, P., 1981. A mathematical model for the prediction of damage in concrete. Cem. Concr. Res. 11, 581-590.

Cowie, J., Glassert, F.P., 1992. The reaction between cement and natural water containing dissolved carbon dioxide. Adv. Cement Res. 14:119–134.

Darabi, M.K., Abu, R.K., Little, D.N., 2012. A Continuum damage mechanics framework for modelling micro-damage healing. Int. J. Solids Struct. 49, 492–513.

Dong, B., Fang, G., Wang, Y., Liu, Y., Hong, S., Zhang, J., Lin, S., Xing, F., 2017. Performance recovery concerning the permeability of concrete by means of a microcapsule based self-healing system. Cem. Concr. Compos. 78, 84–96.

Edvardsen, C., 1999. Water permeability and autogenous healing of cracks in concrete. ACI Mater. J. 96, 448–454.

Garcia Calvo, J.L., Perez, G., Carballosa, P., Erkizia, E., Gaitero, J.J., Guerrero, A., 2017. Development of ultra-high performance concretes with self-healing micro/nano-additions. Constr. Build. Mater. 138, 306–315.

Granger, S., Loukili, A., Pijaudier-Cabot, G., Chanvillard, G., 2007. Experimental characterization of the self-healing of cracks in an ultra high performance cementitious material: mechanical tests and acoustic emission analysis. Cem. Concr. Res. 37, 519-527.

Gupta, S., Pang, S.D., Kua, H.W., 2017. Autonomous healing in concrete by bio-based healing agents A review. Constr. Build. Mater. 146, 419–428.

Hilloulin, B., Grondin, F., Matallah, M., Loukili, A., 2014. Modelling of autogenous healing in ultrahigh performance concrete. Cem. Concr. Res. 61–62, 64-70.

Honma, D., Mihashi, H., Mizukami, T., Nishiwaki, T., 2009. Experimental

study on the self-healing capability of fiber reinforced cementitious composites. In: Tanabe et al. (Eds.), Creep, Shrinkage and Durability Mechanics of Concrete and Concrete Structures. Taylor and Francis Group, pp. 769786.

Huang, H., Ye, G., Damidot, D., 2013. Characterization and quantification of self-healing behaviors of microcracks due to further hydration in cement paste, Cem. Concr. Res. 52, 71-81.

Hughes, T.J.R., 2000. The Finite Element Method: Linear Static and Dynamic Finite Element Analysis, second edition. McGraw-Hill, New York.

Jacobsen, S., Marchand, J., Gerard B., 1998. Concrete Cracks I: Durability and Self-Healing - A Review. In: Proceedings concrete under severe conditions II. London: E and FN Spon, 217–231.

Joseph, C., Gardner, D., Jefferson, T., Isaacs, B., Lark, B., 2011. Self-healing cementitious materials: a review of recent work. Constr. Mater. 164, 29-41.

Kachanov, L., 1958. Continuum model of medium with cracks. J. Eng. Mech. Div. 106, 1039–1051.

Kenneth, R.L., Floyd, O.S., 1956. Autogenous Healing of Cement Paste. J. Proc. 52:1083–1098.

Kim, S.M., Abu Al-Rub, R.K., 2011. Meso-scale computational modeling of the plastic-damage response of cementitious composites. Cem. Concr. Res. 41, 339-358.

Lai, J., Wei, Sun, 2009. Dynamic behaviour and visco-elastic damage model of ultrahigh performance cementitious composite. Cem. Concr. Res. 39, 1044-1051.

Lemaitre, J., Chaboche, J.L., 1990. Mechanics of Solid Materials. Cambridge University Press. Cambridge.

Lepech, M.D., Li, V.C., 2009. Water permeability of engineered cementitious composites. Cem. Concr. Compos. 31, 744-753.

Li, V.C., 1998. ECC-tailored composites through micromechanical modeling fiber reinforced concrete: present and the future. In: Banthia N et al, editors. Fiber Reinforced Concrete: Present and the Future. Canadian Society of Civil Engineers. Montreal, 64.

Li, V.C., Wang, S., Wu, C., 2001. Tensile strain-hardening behavior of PVA-ECC. ACI Mater. J. 98:483–492.

Li, V.C., 2003. On Engineered Cementitious Composites (ECC) - A review of the material and its applications. J. Adv. Concr. Technol. 1, 215–230.

Li, V.C., Yang, E.H., 2007a. Self Healing Materials: An Alternative Approach to 20 Centuries of Materials Science. Springer, the Netherlands.

Li, V.C., Yang, E., 2007b. Self-healing in concrete materials. In: van der Zwaag S, editor. Self-healing materials. Springer, Dordrecht.

Loland, K.E., 1980. Continuous damage model for load-response estimation of concrete. Cem. Concr. Res. 10, 395-402.

Ma, H., Qian, S., Zhang, Z., 2014. Effect of self-healing on water permeability and mechanical property of Medium-Early-Strength Engineered Cementitious Composites. Constr. Build. Mater. 68, 92-101.

Miao, S., Wang, M.L., Schreyer, H.L., 1995. Constitutive models for healing of materials with application to compaction of crushed rock-salt. J. Eng. Mech. 121, 1122-1129.

Neville, A., 2002. Autogenous healing - a concrete miracle?. Concr. Int. 24,76–82.

Qian, S.Z., Zhou, J., Schlangen, E., 2010. Influence of curing condition and precracking time on the self-healing behavior of engineered cementitious composites. Cem. Concr. Compos. 32, 686-693.

Rabotnov, Y.N., 1969. Creep Problems in Structural Members. North-Holland PubCo, Amsterdam, London.

Reddy, J.N., 1993. An Introductory Course to the Finite Element Method, second edition. McGraw-Hill, Boston.

Redon, C., Chermant, J.L., 1999. Damage mechanics applied to concrete reinforced with amorphous cast iron fibers, concrete subjected to compression. Cem. Concr. Compos. 21, 197-204.

Reinhardt, H.W., Jooss, M., 2003. Permeability and self-healing of cracked concrete as a function of temperature and crack width. Cem. Concr. Res. 33, 981-985.

Remmers, J.C., de Borst, R., 2008. Numerical modelling of self healing mechanisms, In: S. van der Zwaag (Ed.), Self Heal. Mater. SE - 17, Springer, Netherlands.

Sahmaran, M., Li, V.C., 2009. Durability properties of micro-cracked ECC containing high volumes fly ash. Cem. Concr. Res. 39, 1033-1043.

Sanz-Herrera, J.A., Boccaccini, A.R., 2011. Modelling bioactivity and degradation of bioactive glass based tissue engineering scaffolds. Int. J. Solids Struct. 48, 257-268.

Schlangen, E., 2010. Fracture mechanics CT2146 Lecture Notes In: Hua X Self-healing of Engineered Cementititous Composites (ECC) in concrete repair system. Master thesis. Delft University of Technology.

Seifan, M., Samani, A.K., Berenjian, A., 2016. Bioconcrete: next generation of self-healing concrete. Appl. Microbiol. Biotech. 100, 2591–2602.

Tao, X., Phillips, D.V., 2005. A simplified isotropic damage model for concrete under bi-axial stress states. Cem. Concr. Compos. 27, 716-726.

van Tittelboom, K., Gruyaert, E., Rahier, H., Nele De Belie, N., 2012. Influence of mix composition on the extent of autogenous crack healing by continued hydration or calcium carbonate formation. Constr. Build. Mater. 37, 349-359.

Wiktor, V., Jonkers, H.M., 2011. Quantification of crack-healing in novel bacteria based self-healing concrete. Cem. Concr. Compos. 33, 763-770.

Yang, Y., Lepech, M.D., Yang, E.H., Li, V.C., 2009. Autogenous healing of engineered cementitious composites under wet-dry cycles. Cement Concrete Res. 39:382–390.

Yang, Y., Yang, E.H., Li, V.C., 2011. Autogenous healing of engineered cementitious composites at early age. Cem. Concr. Res. 41, 176-183.

Zienkiewicz, O.C., Taylor, R.L., 2000. The Finite Element Method, fifth edition. Butterworth–Heinemann, Oxford.